Bitcoin and Global Financial Stress: A Copula-Based Approach to Dependence and Causality-in-Quantiles

Elie Bouri[a], Rangan Gupta[b], Chi Keung Marco Lau[c], David Roubaud[d], Shixuan Wang[e]

[a]USEK Business School, Holy Spirit University of Kaslik, Jounieh, Lebanon, Email: *eliebouri@usek.edu.lb*.

[b]Department of Economics, University of Pretoria, Pretoria, 0002, South Africa, Email: *rangan.gupta@up.ac.za*.

[c]Newcastle Business School, Northumbria University, Newcastle, UK, *Email: chi.lau@northumbria.ac.uk*.

[d]Energy and Sustainable Development (ESD), Montpellier Business School, Montpellier, France, Email: *d.roubaud@montpellier-bs.com*.

[e]Cardiff Business School, Cardiff University, CF10 3EU, United Kingdom, Email: *wsx423104361@gmail.com*.

Corresponding author:

Elie Bouri

USEK Business School, Holy Spirit University of Kaslik, Jounieh, Lebanon. POBOX 446, Jounieh, Lebanon. Phone: +961900861. Email: *eliebouri@usek.edu.lb*.

Abstract

We apply different techniques and uncover the quantile conditional dependence between the global financial stress index and Bitcoin returns from March 18, 2011, to October 7, 2016. The results from the copula-based dependence show evidence of right-tail dependence between the global financial stress index and Bitcoin returns. We focus on the conditional quantile dependence and indicate that the global financial stress index strongly Granger-causes Bitcoin returns at the left and middle tail of the distribution of the Bitcoin returns, conditional on the global financial stress index. Finally, we use a bivariate cross-quantilogram approach and show only limited directional predictability from the global financial stress index to Bitcoin returns in the medium term, for which Bitcoin can act as a safe haven against global financial stress.

2 Research background

Bitcoin is an innovative peer-to-peer electronic payment network that uses a cryptography protocol to secure transactions. The building block of the network relies on an underlying blockchain technology that records and secures all Bitcoin transactions. Blockchain is a distributed ledger made of an unchangeable chain of data blocks spread across multiple sites but chained together cryptographically. Accordingly, trust in Bitcoin is distributed to a large network and established through mass collaboration without a powerful third party. This crucial feature means that unlike conventional fiat currencies, for which the power of authentication and transaction settlement rests with a powerful and centralized government or institution, Bitcoin operates in the absence of a central authority, and its production is neither centralized nor subject to inflation (Ciaian and Rajcaniova, 2016). Instead, Bitcoin production is dictated by the protocol that limits the number of Bitcoin in circulation to 21 million. Although Bitcoin can be produced as a reward for approving Bitcoin transactions in a process called "mining", Bitcoin can also be bought and sold against conventional currencies on trading platforms or exchanges. Although Bitcoin was first designed to allow users to send and receive payments on a peer-to-peer basis, its popularity as an investment asset has considerably increased as speculators and investors store Bitcoin with the objective of increasing its scarcity and potentially driving increases in its value, which has quickly increased from less than one USD in April 2011 to more than one thousand US dollars in March 2017. At the end of March 2017, Bitcoin's market value reached 16.914 billion US dollars, based on a closing price of 1041.06 US dollars[1].

In addition to its exponential price appreciation, Bitcoin has shown strong resilience during periods of stress, suggesting its potential hedging ability against global stress. Weber (2014) and Bouri et al. (2017a) argue that the global uncertainty that accompanied and followed the 2008 global financial crisis facilitated the rapid emergence of Bitcoin as both a financial asset and an alternative currency to conventional economies. Importantly, later stress periods such as the European sovereign debt crisis of 2010-2013 and the Cypriot banking crisis of 2012-2013 have further driven the use of Bitcoin as a shelter from sovereign and systematic risk (Bouri et al., 2017a). Luther and Salter (2017) show that interest in Bitcoin substantially increased following the March 16, 2013, announcement that Cyprus would accept a bailout. Increasing interest in

---

[1] https://coinmarketcap.com/currencies/bitcoin/.

Bitcoin has also been reported in countries such as Greece and Spain, whose banks are troubled. Bitcoin is an alternative to sovereign currencies and is often considered part of an alternative economy. In an environment of high uncertainty and low trust, investors move away from main-state economies and often resort to Bitcoin (Bouri et al., 2017b). Bitcoin has been referred to as digital gold (Popper, 2015), and Dyhrberg (2016a) situates its hedging capability somewhere between gold and the US dollar. Several empirical studies have noted the valuable role of Bitcoin as an investment and have highlighted the diversification benefits of adding Bitcoin to an equity portfolio. Brière et al. (2015) use weekly data from 2010 to 2013 and highlight the low correlation of Bitcoin with both traditional assets (worldwide stocks, bonds, and hard currencies) and alternative investments (commodities, hedge funds, and real estate). The authors note Bitcoin's significant diversification benefits despite its extremely high average return and volatility. Dyhrberg (2016b) shows that Bitcoin is useful as a hedge for UK currency and equities. Bouri et al. (2017b) indicate that Bitcoin can serve as an effective diversifier for major world stock indices, bonds, oil, gold, the general commodity index and the US dollar index. Those authors also reveal that Bitcoin has hedging and safe-haven properties against Asian Pacific and Chinese stocks. Ji et al. (2017) show that Bitcoin is isolated from the conventional global financial system. Bouri et al. (2017c) note the safe-haven property of Bitcoin against equities and reveal that Bitcoin is negatively related to the US VIX. However, the relation between Bitcoin and global financial stress has been ignored. To the best of our knowledge, the only work closely related to this study was conducted by Bouri et al. (2017a), who examine Bitcoin's hedging ability against global uncertainty, as measured by the VIXs of developed and emerging markets. After decomposing Bitcoin returns into different frequencies and applying quantile-on-quantile regressions, the authors show that Bitcoin does act as a hedge against global uncertainty at both the lower and the upper ends of Bitcoin returns and global uncertainty, particularly on shorter investment horizons. Although Bouri et al. (2017a) differentiate between short and long investment horizons and between upper and lower quantiles, they ignore the dependence structure, as captured by copula, along with Granger-causality in both distributions and quantiles. Furthermore, Bank of America Merrill Lynch recently introduced an index for global financial distress that better captures global stress than the VIX[2]. Released in November 2010, the so-

---

[2] http://uk.reuters.com/article/markets-stressindex-idUSN2920764420101129.

called global financial stress index (GFSI) aggregates 23 measures of stress covering three types of financial market stress (risk, hedging demand, and investor (flows in the financial system) appetite for risk) across five asset classes (credit, equity, interest rates, forex and commodity markets) and various geographies. Bank of America Merrill Lynch argues that the breadth and depth of the GFSI make it a more accurate gauge of global stress than the VIX, which is based on option data. More specifically, the GFSI helps detect significant market turning points, as indicated by the back-testing that has shown the high degree of the GFSI's accuracy in forecasting market sell-offs since 2000. Based on the above, it appears that the GFSI is an essential tool for market participants to make better investment and risk management decisions. Importantly, the increased knowledge of which risks are essential and against which to hedge them in the different quantiles whilst explaining the copula dependence structure are two crucial aspects of successful investing. It follows that the safe-haven property of Bitcoin against this global measure of market stress requires a thorough examination using newly developed techniques. Therefore, in this study, we examine the dependence between Bitcoin returns and the GFSI using the copula function and the Granger causality in both distribution and quantiles from a predictive perspective. Our sample period spans from March 18, 2011, to October 7, 2016.

Whereas some recent studies on the economics of Bitcoin have applied the Granger causality test in the conditional mean or in conditional variance (e.g., Blacilar et al., 2017), this study applies a copula-based approach to uncover the conditional dependence and causality in the quantiles between Bitcoin and global financial stress. Instead of considering the contemporaneous causality relationships, we adopt two predictive approaches in the Granger causality rationale. The first is the out-of-sample approach of Hong and Li (2005), which captures the Granger causality in distributions in each conditional quantile. The second is the cross-quantilogram approach by Han et al. (2016), which allows the measure of directional predictability in quantiles from the GFSI to Bitcoin returns.

The contributions of this study are three-fold. First, in contrast to Bouri et al. (2017a), we use a broader measure of global financial stress that captures, in addition to the VIX, a variety of market stresses (risk, hedging demand, and investor appetite for risk) across five asset classes (credit, equity, interest rates, forex and commodity markets) and various geographies. Second, for the first time, we uncover the dependence between the GFSI and Bitcoin returns across the entire range of quantiles using the copula function and Granger causality tests in each conditional

quantile[3]. These combinations between copula and quantile causality enable us to uncover the Granger causality in both distributions and quantiles. Third, instead of examining the contemporaneous causality relationships, we adopt a predictive approach in the Granger causality rationale (Han et al., 2016).

A quantile dependence analysis enriches our understanding of the ability of Bitcoin to act as a safe haven against global financial stress. We first use a copula function and report evidence of right-tail dependence between the GFSI and Bitcoin returns. We also derive the conditional quantile from the inverse function of a conditional distribution function and show that the GSFI strongly Granger-causes Bitcoin returns at the left tail (i.e., during very deficient performance) and the middle (i.e., during average performance) but not at the right tail (i.e., during very robust performance) of the distribution of the Bitcoin returns conditional on the GSFI. Importantly, we consider a quantile-to-quantile analysis from a predictive perspective and find that when global financial stress is very high (above the upper 90th quantile), there is a very large positive gain in the price of Bitcoin for approximately 60 days. Specifically, the GFSI has a very large positive gain for the next 60 days. This significant directional predictability from the GFSI to Bitcoin return indicates that Bitcoin can act as a safe haven against global financial stress from a medium-term perspective. Our findings are important to practitioners, scholars and policy-makers.

2 Data

The data used in this study are daily (5 days per week) and cover the period from March 18, 2011, to October 7, 2016. The data consist of Bitcoin prices and the GFSI. The prices are collected from CoinDesk (www.coindesk.com/price) and represent the average price of Bitcoin across leading exchanges (Bouri et al., 2017a). The GFSI, which is collected from the Bloomberg Terminal, captures global financial stress. Levels greater than zero indicate more financial market stress than normal, and vice-versa. Table 1 shows the summary statistics of the GFSI and the return on Bitcoin (RBC) (calculated as the difference in logarithm between two consecutive prices). There are several noteworthy observations. The GFSI and RBC both have positive means. The GFSI has a larger standard deviation than does the RBC return. The GFSI

---

[3] Balcilar et al. (2017) apply a quantiles-based approach but only consider the Granger causality in the quantiles between trading and Bitcoin returns/volatility.

and RBC both are positively skewed. RBC has significant excess kurtosis, whereas the GFSI has minimal kurtosis. The JB test shows that the GFSI and RBC are not following a normal distribution. The GFSI and RBC are negative correlated (-0.048).

Table 1. Summary statistics.

Series	GFSI	RBC
Mean	0.115	0.005
Max	1.310	0.500
Min	-0.530	-0.444
SD	0.385	0.064
Skew	0.772	0.106
Kurtosis	3.257	13.668
JB_test	148.134	6883.549
Correlation	-0.048	

3 Methods and results

There are three advantages of using copulas in analyzing the dependence. First, the copula method is designed to capture the complex and non-linear dependence structure of a multivariate distribution, whilst the traditional Pearson correlation assumes a linear dependence relationship and is not capable of measuring the asymmetric dependence. Copulas enable us to find both the tail dependence and the asymmetric dependence. Importantly, the tail dependence can measure the probability of simultaneous extreme losses for investors. Second, the marginal behaviour and the dependence structure are separated by the framework of copulas. This separation facilitates both the model specification and the model estimation. Compared with univariate models, the flexibility of the multivariate models is limited. Copulas can jointly combine different univariate models through their copula functions. The estimation can be performed in separate steps for the marginal models and the copula functions. Finally, copulas are invariant to increasing and continuous transformations (Ning, 2010), such as the scaling of logarithm returns, which is commonly used in economic and finance studies.

Nevertheless, the above copula dependence model does not provide a conclusion about the causality between variables. Thus, once we identify the appropriateness of adopting copula models, we proceed further to uncover the causality dynamic between the GFSI and RBC by computing the quantile forecasts that rely on the inversion of the parametric conditional copula distribution. We use the model by Lee and Yang (2014) to examine the dependence between the GFSI and RBC using a parametric copula because the linear Granger causality test cannot model

7

the asymmetric dependence between the GFSI and RBC, possibly because of the existence of nonlinearity and structural breaks. From the modelling perspective, it is more informative to explore the causal relationship between the GFSI and RBC using the Granger causality in distribution (GCD) test, which can model the causal relation at the extremes of the return distributions rather than only at the centre. For market practitioners, it is more realistic to imagine that causality is only anticipated at high quantiles of the GFSI and RBC, because RBC may act as a safe haven when the global financial market panics. Indeed, this hypothesis is supported by the empirical evidence we provide later.

Finally, we employ the recent directional predictability test of Han et al. (2016) to complement the GCD test because investors may want to use the GFSI to predict the movement of RBC; this follows the need to access the forecasting performance of RBC using the GFSI as a predictor. The null hypothesis is that the GFSI has no directional predictability for another time series. The added advantage of the cross-quantilogram of Han et al. (2016) over GCD is its ability to detect the magnitude, duration, and direction of the relationship between the GFSI and RBC spontaneously, whilst GCD failed to do so. Another advantage is that the model allows us to select arbitrary quantiles for both the GFSI and RBC, rather than pre-set quantiles for GCD; furthermore, the use of the bootstrap technique allows for the use of large lags in the directional predictability test.

3.1 Copula dependence model

A copula is a multivariate cumulative distribution function, and its marginal distributions are uniform on the interval [0, 1]. Nelsen (1999) review the rigorous mathematical foundation of copulas. Sklar's theorem plays the central role in the theory of copulas. "Sklar's theorem elucidates the role that copulas play in the relationship between multivariate distribution functions and their univariate margin" (Nelsen, 1999).

Sklar's Theorem. Let F_{XY} be a joint distribution function. F_{XY} has two marginal distributions F_X and F_Y. There exists a copula C such that all x, y in **R**,

$$F_{XY} = C(F_X(x), F_Y(y))$$

The copula C is unique if marginal distributions F_X and F_Y are continuous; otherwise, C is uniquely determined on $Ran(F_X) \times Ran(F_Y)$. Sklar's theorem enables us to model the

8

marginal distributions and the dependence structure separately. Within our context, a bivariate joint cumulative distribution function of returns of Bitcoin and the GFSI can be decomposed into two marginal cumulative distribution functions and a copula cumulative distribution function.

Assuming F_X and F_Y are differentiable, the bivariate joint density is defined as

$$f_{XY} = \frac{\partial^2 F_{XY}}{\partial x \partial y} = f_X(x) f_Y(y) c(u,v)$$

where u and v are the "probability integral transforms" of x and y based on $F_X(x)$ and $F_Y(y)$, respectively. $f_X(x)$ and $f_Y(y)$ are marginal densities of x and y, respectively, and $c(u,v) = \partial^2 C(u,v)/\partial u \partial v$ is the copula density. Therefore, the bivariate joint density is expressed as the product of the two marginal densities and the copula density.

One particularly important dependence measure that copula can capture is the tail dependence, which measures the probability that two variables are jointly in their lower or upper tails. Tail dependence can be viewed as a pronounced spike in the data points in the plot of the lower-left or upper-right corner of a copula probability density. Intuitively, lower or upper-tail dependence is a relatively high probability density in the lower or upper quantile of the joint distribution. In Nelsen (1999), the left and right-tail dependence coefficients of a copula are defined as

$$\varphi_L = \lim_{u \to 0} \mathbf{P}\left[Y \le F_Y^{(-1)}(u) \mid X \le F_X^{(-1)}(u)\right] = \lim_{u \to 0} \frac{C(u,u)}{u}$$

$$\varphi_R = \lim_{u \to 1} \mathbf{P}\left[Y > F_Y^{(-1)}(u) \mid X > F_X^{(-1)}(u)\right] = \lim_{u \to 1} \frac{1 - 2u + C(u,u)}{1 - u}$$

where C is a copula function. (1)

3.1.1 Marginal models

Specifying the correct marginal models is a key step. With incorrect marginal models, the estimated copula model is unable to capture the correct dependence structure of two series. The Q-statistic and the Q^2-statistic are applied to examine the hypothesis of no serial correlation in the estimated standardized residuals. The ARCH-LM statistic is employed to ensure that no heteroscedasticity is in the estimated standardized residuals.

3.1.2 Estimation methods

The quasi-maximum likelihood method (Bollerslev and Wooldridge, 1992) is applied to estimate the marginal models. The variance-covariance matrix of the estimated coefficients is adjusted accordingly. We use the Canonical Maximum Likelihood method to transform the standardized residuals, which are based on a cumulative distribution function (CDF)[4], into uniform distribution. We present the parametric copulas used in the paper and their tail-dependence properties.

Normal Copula

$$C_N(u,v) = \Phi_\rho(\Phi^{-1}(u), \Phi^{-1}(v)) \tag{2}$$

where $\Phi^{-1}(\bullet)$ is the inverse of the distribution function of a standard normal random variable, and $\Phi_\rho(\bullet)$ denotes the distribution function of a bivariate normal random vector with zero means and correlation ρ. A normal copula has zero tail dependence.

Clayton Copula

$$C_C(u,v) = \left[\max(u^{-\theta} + v^{-\theta} - 1, 0) \right]^{-1/\theta}, \text{ where } \theta \in [-1, \infty) \setminus \{0\} \tag{3}$$

The Clayton copula has zero upper-tail dependence but positive lower-tail dependence.

Rotated Clayton Copula

$$C_{RC}(u,v) = \left[\max((1-u)^{-\theta} + (1-v)^{-\theta} - 1, 0) \right]^{-1/\theta}, \text{ where } \theta \in [-1, \infty) \setminus \{0\} \tag{4}$$

The rotated Clayton copula has zero lower-tail dependence but positive upper-tail dependence.

Plackett Copula

$$C_P = \frac{1 + (\theta-1)(u+v) - \sqrt{[1 + (\theta-1)(u+v)]^2 - 4\theta(\theta-1)uv}}{2(\theta-1)}, \text{ where } \theta \in (0, \infty) \tag{5}$$

The Plackett copula has zero tail dependence.

Frank Copula

$$C_F(u,v) = -\frac{1}{\theta} \ln \left(1 + \frac{(e^{-\theta u} - 1)(e^{-\theta v} - 1)}{e^{-\theta} - 1} \right), \text{ where } \theta \in (-\infty, \infty) \setminus \{0\} \tag{6}$$

The Frank copula has zero tail dependence.

Gumbel Copula

---

[4] The empirical marginal cumulative distribution function is computed by $\hat{F}_k(x) = \frac{1}{T+1} \sum_{t=1}^{T} \mathbf{I}(\eta_{k,t} \le x)$, where $\mathbf{I}$ ($\bullet$) is an indicator function.

$$C_G(u,v) = \exp\left(-\left[(-\ln u)^\theta + (-\ln v)^\theta\right]^{1/\theta}\right), \text{ where } \theta \in [1,\infty) \qquad (7)$$

The Gumbel copula has zero lower-tail dependence but positive upper-tail dependence.

Rotated Gumbel Copula

$$C_{RG}(u,v) = \exp\left(-\left[(-\ln(1-u))^\theta + (-\ln(1-v))^\theta\right]^{1/\theta}\right), \text{ where } \theta \in [1,\infty) \qquad (8)$$

The rotated Gumbel copula has zero upper-tail dependence but positive lower-tail dependence.

Student's t Copula

$$C_{ST}(u,v) = \Psi_\rho(\Psi^{-1}(u,\upsilon), \Psi^{-1}(v,\upsilon), \upsilon) \qquad (9)$$

where $\Psi_\rho(\bullet)$ is the distribution function of a bivariate Student's t distribution with correlation ρ and degree of freedom parameter υ, and Ψ^{-1} is the inverse of the distribution function for the univariate Student's t distribution with zero means and degree of freedom υ. The Student's t copula has symmetric tail dependence.

Symmetrised Joe-Clayton Copula

$$C_{SJC}(u,v) = 0.5\left(C_{JC}(u,v) + C_{JC}(1-u,1-v) + u + v - 1\right) \qquad (10)$$

where

$$C_{JC}(u,v) = 1 - \left(1 - \left\{\left[1-(1-u)^\kappa\right]^{-\gamma} + \left[1-(1-v)^\kappa\right]^{-\gamma} - 1\right\}^{-1/\gamma}\right)^{1/\kappa}$$

$$\kappa = 1/\log_2(2-\tau^U)$$

$$\gamma = -1/\log_2(\tau^L)$$

and $\tau^U, \tau^L \in (0,1)$ \qquad (11)

Table 2 shows the probability density of the empirical copula with the number of observations at 1451 (trading days) from March 18, 2011, to October 7, 2016. We rank the pair of series in ascending order and then divide each series evenly into 10 bins. Bin 10 includes the observations with the highest values, and bin 1 includes observations with the lowest values. The ranks for the GFSI (i) are on the vertical axis, whilst the ranks for RBC (j) are on the horizontal axis. For the vertical axis, observations increase from the bottom to the top. For the horizontal axis, observations increase from left to right. Cell (1,1) is located on the lower-left corner, cell (10,1) is located on the lower-right corner, cell (10,10) is located on the upper-right corner, and cell (1,10) is located on the upper-left corner. The number of observations in cell (1,1) reveals information about a positive left-tail dependence, the number of observations in cell (1,10)

11

reveals information about a negative right-tail dependence, the number of observations in cell (10,10) reveals information about a positive right-tail dependence, and the number of observations in cell (10,1) reveals information about a negative left-tail dependence between the two states. There are several noteworthy observations: cell (1, 1) has a low number, and there is no positive left-tail dependence (see lower-left corner, Table 2). When the global financial markets are generally healthy, it is unlikely that we will observe an extreme decrease in the Bitcoin market. Cell (10,1) has a high number, and there is strong negative left-tail dependence (lower-right corner, Table 2). This finding indicates that the Bitcoin market is prosperous when the GFSI is very low. Cell (1, 10) has a high number, and there is strong negative right-tail dependence (upper-left corner, Table 2). Investors must rationally manage risks under this scenario, in which an extremely stressed financial market and a substantial decrease in the Bitcoin market occur simultaneously. An extreme joint loss is likely to be higher than a normal value-at-risk (VAR). Cell (10, 10) has a high number, and there is strong positive right-tail dependence (upper-right corner, Table 2). It is interesting to observe that the Bitcoin market can perform well when the global financial markets are in depression. This evidence justifies that Bitcoin provides a channel against global financial stress.

Table 2. Empirical copula for the GFSI and Bitcoin return.

	Bitcoin-lowest									Bitcoin-highest
GFSI-highest	26	20	11	8	10	5	12	13	15	25
	11	17	18	20	19	21	13	12	11	7
	9	8	13	13	24	23	23	12	10	12
	17	13	19	10	13	12	18	11	15	16
	16	13	12	17	15	9	15	18	21	17
	10	14	18	15	18	16	12	13	14	4
	13	15	21	13	12	22	19	15	18	11
	12	15	16	17	9	13	7	17	7	19
	26	14	8	19	14	12	16	15	18	10
GFSI-lowest	5	16	9	13	11	13	10	19	16	24

Notes: We rank the pair of returns in ascending order and then divide each series evenly into 10 bins. Bin 10 includes the observations with the highest values, and bin 1 includes observations with the lowest values. The ranks for the return of Bitcoin (i) in the pair are on the vertical axis, whilst the ranks for the GFSI (j) in the pair are on the horizontal axis. For the vertical axis, returns increase from the bottom to the top. For the horizontal axis, returns increase from left to right.

The ARMA(1,1)-tGARCH(1,1) model has been chosen for the marginal model as shown in Table 3. There are three motivations to use this model. First, our data contain a serial correlation. The level equation is chosen to be ARMA (1,1). Second, our data have heteroscedasticity. The volatility equation is chosen to be GARCH (1,1). Third, there are many outliers in the data. The standardized residuals follow the Student-t distribution. The order of ARMA is (1,1) and the order of GARCH is (1,1), which is sufficient for our data with evidence from the autocorrelation and heteroscedasticity tests. This model is parsimonious, which can capture both autocorrelation and heteroskedasticity[5]. The model is shown as follows:

$$R_{k,t} = \alpha_{k,0} + \alpha_{k,1}R_{k,t-1} + \alpha_{k,2}\varepsilon_{k,t-1} + \varepsilon_{k,t} \qquad k = 1, 2$$

$$h_{k,t} = \beta_{k,0} + \beta_{k,1}\varepsilon_{k,t-1}^2 + \beta_{k,2}h_{k,t-1}$$

$$\eta_{k,t} = \varepsilon_{k,t} \Big/ \sqrt{h_{k,t}} \qquad\qquad \eta_{k,t} \mid \Omega_{t-1} \sim t(\upsilon_k) \qquad (12)$$

where $\eta_{k,t}$ is the standardized residuals, which follows the Student-t distribution with υ_k degrees of freedom. The ARMA(1,1)-tGARCH(1,1) model is estimated by the quasi-maximum likelihood method.

Table 3. Estimation of marginal models.

		GFSI		RBC	
		Est Coef	**t Stat**	**Est Coef**	**t Stat**
	Constant	-0.002	-2.098	0.000	1.516
ARMA(1,1)	**AR{1}**	0.991	363.997	0.944	30.330
	MA{1}	0.175	6.505	-0.918	-24.659
	Constant	0.000068	2.944	0.000075	4.082
GARCH(1,1)	**GARCH{1}**	0.846	26.445	0.770	33.477
	ARCH{1}	0.110	4.597	0.230	5.492
Residual	**DoF**	5.087	6.815	2.977	13.404
		Test Stat	**P-Value**	**Test Stat**	**P-Value**
	Q(5)	4.935	0.424	13.041	0.023
	Q(10)	5.593	0.848	27.605	0.002
Diagnostics	**Q²(5)**	5.043	0.411	2.078	0.838
	Q²(10)	8.998	0.532	4.732	0.908
	Arch(5)	5.076	0.407	2.135	0.830

[5] When k = 1, that is the model for the GFSI; when k = 2, that is the model for the RBC.

Arch(10)	8.579	0.572	4.860	0.900

Notes: The order of ARMA is (1,1), and the order of GARCH is (1,1), which is sufficient for our data with evidence from the autocorrelation and heteroscedasticity tests. This model is parsimonious; it can capture both autocorrelation and heteroskedasticity.

As we can observe from the diagnostics section in Table 3, $Q(P)$ and $Q^2(P)$ are Q-statistics for testing the hypothesis of no serial correlation in the standardized residuals and squared standardized residuals, respectively. ARCH (P) is the LM test for the hypothesis of no autoregressive conditional heteroscedasticity in the standardized residuals. These statistics each have a chi-square distribution with P degrees of freedom. Based on the estimation results, the t stat is significant for all coefficients in the model for both the GFSI and RBC. The Q-statistics suggest no serial correlation in the standardized residuals of GSFI. However, there is serial correlation in the standardized residuals of RBS, as indicated by the p-value of the Q-statistics. The LM test suggests no heteroscedasticity in the standardized residuals of the GSFI and RBC.

Table 4 reports the estimated results for our data by applying nine candidate copulas, including normal, Clayton, Rotated Clayton, Plackett, Frank, Gumbel, Rotated Gumbel, Student's t and Symmetrised Joe-Clayton. In accordance with Patton (2006), we calculate the copula likelihood for each candidate copula. Based on the copula likelihood, we further calculate two information criteria: Akaike information criterion (AIC) and Bayesian information criterion (BIC). Additionally, we compute the tail dependence for each fitted copula. According to the copula log likelihood, the Gumbel copula provides the best fit for our data. According to AIC and BIC, the Gumbel copula is the best model for our data. Only through the Gumbel copula can we find tail dependence in the right tail. All other copulas indicate no tail dependence. The normal copula has zero tail dependence. The Clayton copula has zero upper-tail dependence. The rotated Clayton copula has zero lower-tail dependence. The Plackett copula has zero tail dependence. The Frank copula has zero tail dependence. The Gumbel copula has zero lower-tail dependence. The rotated Gumbel copula has zero upper-tail dependence. The Student's t copula has symmetric tail dependence. The SJC copula parameters are the tail-dependence coefficients, but in reverse order. Overall, the dependence structure of our data would be best captured by the Gumbel copula[6].

---

[6] We also considered the possibility of the regime- dependent copula of Wang et al. (2013). However, the results are insignificant (for details, please see the appendix).

Table 4. Copulas model estimation.

Copula Type	Estimated Parameter		Copula Log Likelihood	AIC	BIC	Left-tail Dependence	Right-tail Dependence
Normal	ρ	0.003	0.007	-0.012	-0.008	0.000	0.000
Clayton	θ	0.000	-0.002	0.005	0.009	0.000	0.000
Rotated Clayton	θ	0.020	0.281	-0.560	-0.557	0.000	0.000
Plackett	θ	1.021	0.034	-0.067	-0.063	0.000	0.000
Frank	θ	0.041	0.034	-0.066	-0.062	0.000	0.000
Gumbel	θ	1.014	0.697	-1.392	-1.388	0.000	0.019
Rotated Gumbel	θ	1.000	-0.003	0.007	0.011	0.000	0.000
Student's t	ρ	0.004	0.267	-0.531	-0.524	0.000	0.000
	υ	49.101					
Symmetrised Joe-Clayton	upper tail	0.000	-0.769	1.542	1.549	0.000	0.000
	lower tail	0.000					

3.2 Granger causality in quantile

From subsection 3.1, we find evidence that tail dependence is in the right tail by the Gumbel copula, whilst all other copulas indicate no tail dependence. Although we identify the Gumbel copula as the appropriate copula for our data, the analysis provides no information about the causality between the GFSI and RBC. Therefore, this section seeks to provide a more informative test to examine the GCD as a tool to explore a causal relationship between the GSFI and the return of Bitcoin (RBC). We apply the proposed out-of-sample test for GCD in accordance with Hong and Li (2005) with the null hypothesis that X_t does not Granger cause Y_t in distribution: H0: c(u, v) = 1, where c(u, v) is the conditional copula density function, with u and v as the conditional probability integral transforms of X_t (i.e., $GSFI_t$) and Y_t (i.e., RBC_t), respectively. The forecasted conditional variance for { X_t } and { Y_t }, $\hat{h}_{x,t+1}$ and $\hat{h}_{y,t+1}$, are computed by

$$\hat{h}_{x,t+1} = \hat{\beta}_{x0} + \hat{\beta}_{x1}x_t^2 + \hat{\beta}_{x2}\hat{h}_{t,x}$$
$$\hat{h}_{y,t+1} = \hat{\beta}_{y0} + \hat{\beta}_{y1}y_t^2 + \hat{\beta}_{y2}\hat{h}_{t,x} \tag{13}$$

The CDF values of $\hat{u}_{t+1}$ and $\hat{v}_{t+1}$ for x_{t+1} and y_{t+1} are calculated by the empirical distribution function (EDF), and a nonparametric copula function is estimated with pared EDF values $\{\hat{u}_{t+1}, \hat{v}_{t+1}\}_{t=R}^{T-1}$ using a quartic kernel function specified as follows:

$$k(u) = \frac{15}{16}(1 - u^2)^2 I(|u| \leq 1) \tag{14}$$

The GCD results using the Hong and Li (2005) test statistic for $\{x_{t+1}, y_{t+1}\}_{t=R}^{T-1}$ is 40.843, which is significant at the 1% level, indicating that there is significant GCD between the GSFI and RBC. However, evidence of the GCD test does not imply Granger causality in each conditional quantile. In our empirical study, we focus on three regions of the distribution: the left tail (1% quantile, 5% quantile and 10% quantile), the central region (40% quantile, median and 60% quantile) and the right tail (90% quantile, 95% quantile and 99% quantile); this is the same as Lee and Yang (2014). The objective is to forecast the conditional quantile, $q_\alpha(Y_t|\mathcal{F}_t)$, where α is the left tail probability. The conditional quantile $q_\alpha(Y_t|\mathcal{F}_t)$ is derived from the inverse function of a conditional distribution function:

$$q_\alpha(Y_t|\mathcal{F}_t) = F_Y^{-1}(\alpha|\mathcal{F}_t) \tag{15}$$

where $F_Y(Y_t|\mathcal{F}_t)$ is the predicted conditional distribution function of Y_t. The inverse is to compute $q_\alpha(Y_t|\mathcal{F}_t)$ from

$$\int_{-\infty}^{q_\alpha(Y_t|\mathcal{F}_t)} f\gamma(y|\mathcal{F}_t)dy = \alpha \qquad (16)$$

where $f\gamma(y|\mathcal{F}_t)$ is the predicted conditional distribution function. The quantile forecasting models $q_\alpha(Y_t|\mathcal{F}_t)$ are computed by solving the equation

$$C_u(F_X(x_{t+1}), F_Y(q_\alpha(Y_t|\mathcal{F}_t))) = \alpha \qquad (17)$$

To evaluate the predictive ability of those quantile forecasting models $q_\alpha(Y_t|\mathcal{F}_t)$ obtained from the seven ($I = 7$) copula functions for C(u; v), we use the "check" loss function of Koenker and Bassett (1978)[7]. The expected check loss for a quantile forecast $q_\alpha(Y_t|\mathcal{F}_t)$ at a given α is

$$Q(\alpha) = E[\alpha - I(Y_t - q_\alpha(Y_t|\mathcal{F}_t) < 0)](Y_t - q_\alpha(Y_t|\mathcal{F}_t)) \qquad (18)$$

We denote the k'th type of copula function as C_k(u; v) (k = 1,…,l = 7). For each copula distribution function C_k(u; v), we also denote the corresponding quantile forecast as $q_{\alpha,k}(Y_t|\mathcal{F}_t)$ and its expected check loss as $Q_k(\alpha)$. To compare copula model 1 (benchmark) and model k (= 2,…,l), we consider the corresponding check loss-differential

$$D_k = Q_1(\alpha) - Q_k(\alpha) \qquad (19)$$

We can estimate D_k by

$$\widehat{D}_{k,p} = \widehat{Q}_{1,p}(\alpha) - \widehat{Q}_{k,p}(\alpha) \qquad (20)$$

where

$$\widehat{Q}_{k,p}(\alpha) = \frac{1}{p}\sum_{t=R}^{T-1} [\alpha - I(Y_t - q_\alpha(Y_t|\mathcal{F}_t) < 0)](Y_t - q_\alpha(Y_t|\mathcal{F}_t)), \qquad k = 1, \dots, l$$

The conditional quantile forecasts from using the copula distribution function C_k (k = 2,…) with the largest value $\widehat{D}_{k,p}$ will be preferred. The results of testing GCQ in p-values are reported in Table 5. The small p-values of the reality check in Table 5 signal the rejection of the null hypothesis, indicating that there is a copula function to model GCQ and produce a better quantile forecast of the RBC by conditioning on the GSFI. We can observe that a quantile forecasting model with no Granger causality in the quantile is rejected in many quantiles, except for the quantile at 60%, 70%, 90%, and 95%, indicating that the GSFI strongly Granger-causes the RBC at the left tail (poor performance) and centre (usual performance) but not at the right tail (superior performance) of the distribution of the RBC conditional on the GSFI.

---

[7] For detailed information, please refer to Lee and Yang (2014).

Table 5. Testing for GCQ.

1%	5%	10%	20%	30%	40%	50%	60%	70%	80%	90%	95%	99%
0	0	0	0	0	0	0	0.346574	0.277259	0.034657	0.207944	0.138629	0.069315

Notes: We compute the quantile forecasts by inverting the parametric conditional copula distribution. We use six copulas (Gaussian, Frank, Clayton, Clayton Survival, Gumbel and Gumbel Survival copulas). The check loss functions are compared to evaluate the predictive ability of different quantile forecasting using different copula models. The benchmark quantile forecasts are computed using the independent copula such that there is no GCQ. Reported are the bootstrap p-values for testing the null hypothesis that none of these six copula models (which model GCQ) produces a better quantile forecast than the independent copula (which gives no GCQ). The small p-values of the reality check indicate the rejection of the null hypothesis, indicating that there is a copula function to model GCQ and produce a better quantile forecast.
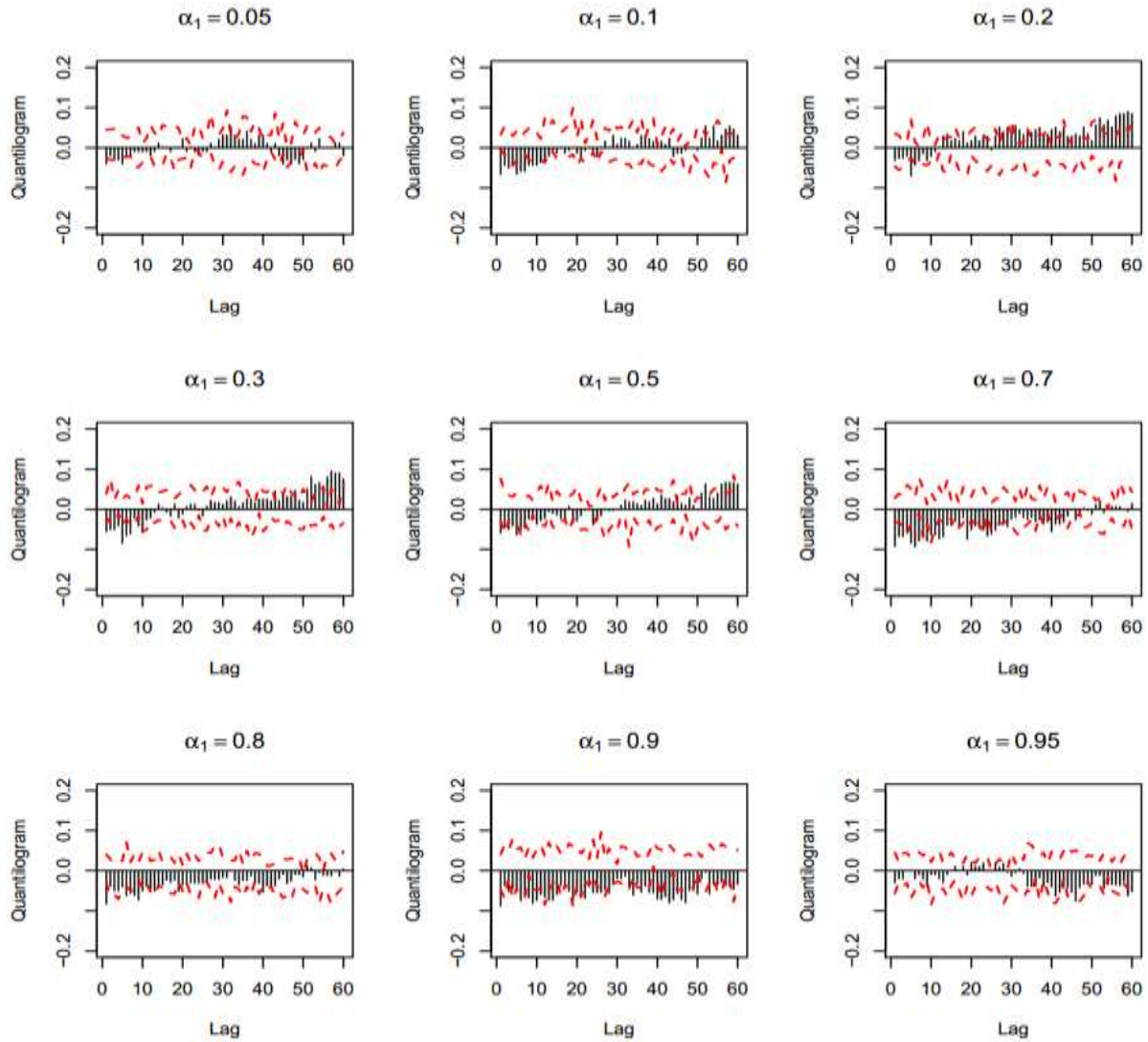
3.3 Cross-quantilogram

In section 3.3, we examined the relationships between the GFSI and RBC at the extremes of the return distributions rather than only at the centre and confirmed the hypothesis that causality between the GFSI and RBC is only anticipated at high quantiles of the GFSI and RBC because RBC may act as a safe haven when the global financial market is in panic. However, we need a complementary analysis to investigate directional predictability because investors may want to use the GFSI to predict the movement of the RBC. As indicated in the previous section, the added advantage of the predictability test over the GCD test is its ability to detect the magnitude, duration, and direction of the relationship between the GFSI and RBC spontaneously such that investors can use this information to inform their trading strategies. Another advantage is that this test allows researchers to select arbitrary quantiles for the GFSI and RBC rather than pre-set quantiles, as in the case of GCD. Furthermore, the use of the bootstrap technique allows for the use of large lags in the directional predictability test. The directional predictability test of Han et al. (2016) was used by Jiang et al. (2016) to investigate the daily, overnight, intraday, and rolling return spillovers of four key agricultural commodities—soybeans, wheat, corn, and sugar—between the U.S. and Chinese futures markets. The authors found the empirical model very useful in capturing the extreme quantiles dependence between markets. Therefore, in this section, we use the cross-quantilogram proposed by Han et al. (2016) to measure the quantile dependence between the GSFI and RBC and to test the null hypothesis that GSFI has no

directional predictability to RBC. The cross-quantilogram can provide a quantile-to-quantile relationship from the GSFI to RBC. The linear quantile regression can be specified as

$$q_{\alpha(\tau_{t+1}|\mathcal{F}_t)} = \beta_{0,\alpha} + \beta_{1,\alpha}x_t + \beta_{2,\alpha}x_t q_\alpha(\tau_t|\mathcal{F}_{t-1}) + \beta_{3,\alpha}|\tau_t| \tag{21}$$

where τ_t and x_t are the RBC and GSFI, respectively, and $q_{\alpha(\tau_{t+1}|\mathcal{F}_t)}$ is the conditional quantile of the RBC given the information $\mathcal{F}_t$ at time t. The cross-quantilogram $\hat{p}_\alpha(k)$ and the portmanteau tests $\hat{Q}_\alpha^{(p)}$ of the Box-Ljung versions are provided in the figures to detect the directional predictability from the RBC to GSFI. For the quantiles of RBC q$_1$ (α$_1$), we consider a wide range for α$_1$ = 0.05, 0.1, 0.2, 0.3, 0.5, 0.7, 0.8, 0.9 and 0.95. For the quantiles of GSFI q$_2$ (α$_2$), we consider a wide range for α$_2$ = 0.1, 0.5, and 0.9. In each graph, we show the 95% bootstrap confidence intervals for no predictability based on 1000 bootstrapped replicates. The maximum lag we consider is 2 months (i.e., k = 60). To estimate the critical values from the limiting distribution, we could use the nonparametric estimation using the stationary bootstrap (SB) of Politis and Romano (1994) . The SB is a block bootstrap method with blocks of random lengths. The SB resample is strictly stationary, conditional on the original sample. Alternatively, we can apply the self-normalized approach proposed in Lobato (2001) to test the absence of autocorrelation of a time series that is not necessarily independent. A key ingredient of the self-normalized statistic is an estimate of cross-correlation based on subsamples.

Figs. 1(a) and 1(b) are for the case when the stock variance is in the lower quantile, i.e., q2 (α$_2$) for α$_2$ = 0.1. The cross-quantilogram $\hat{p}_\alpha(k)$ for α$_1$ = 0.2 is positive and significant after the second week. This finding means that when GSFI is very low, there is less likely to be a very large negative loss for Bitcoin. The cross-quantilogram p^_α (k) for α$_1$ = 0.7 and 0.9 is negative and significant for most lags, indicating that when GSFI is very low, it is less likely to have a very large positive gain for Bitcoin. Fig. 1(b) shows that the Box-Ljung test statistics are significant for quantiles α$_1$ =0.1, 0.2, 0.3, 0.7 and 0.9.
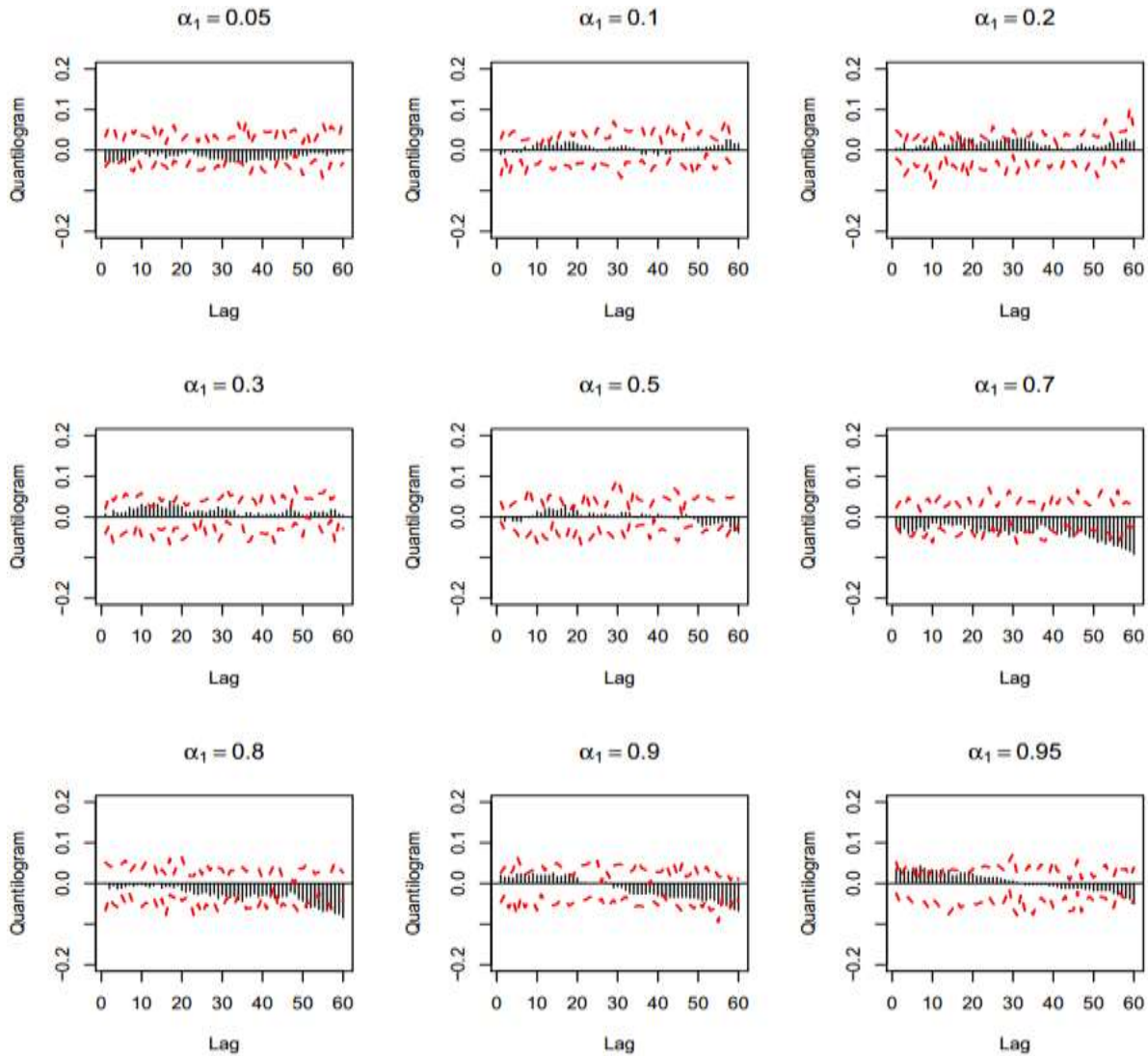
Fig. 1(a). The sample cross quantilogram $\hat{p}_\alpha(k)$ for α2 = 0.1 to detect directional predictability from the GSFI to RBC. Bar graphs describe sample cross quantilograms, and lines are the 95% bootstrap confidence intervals.
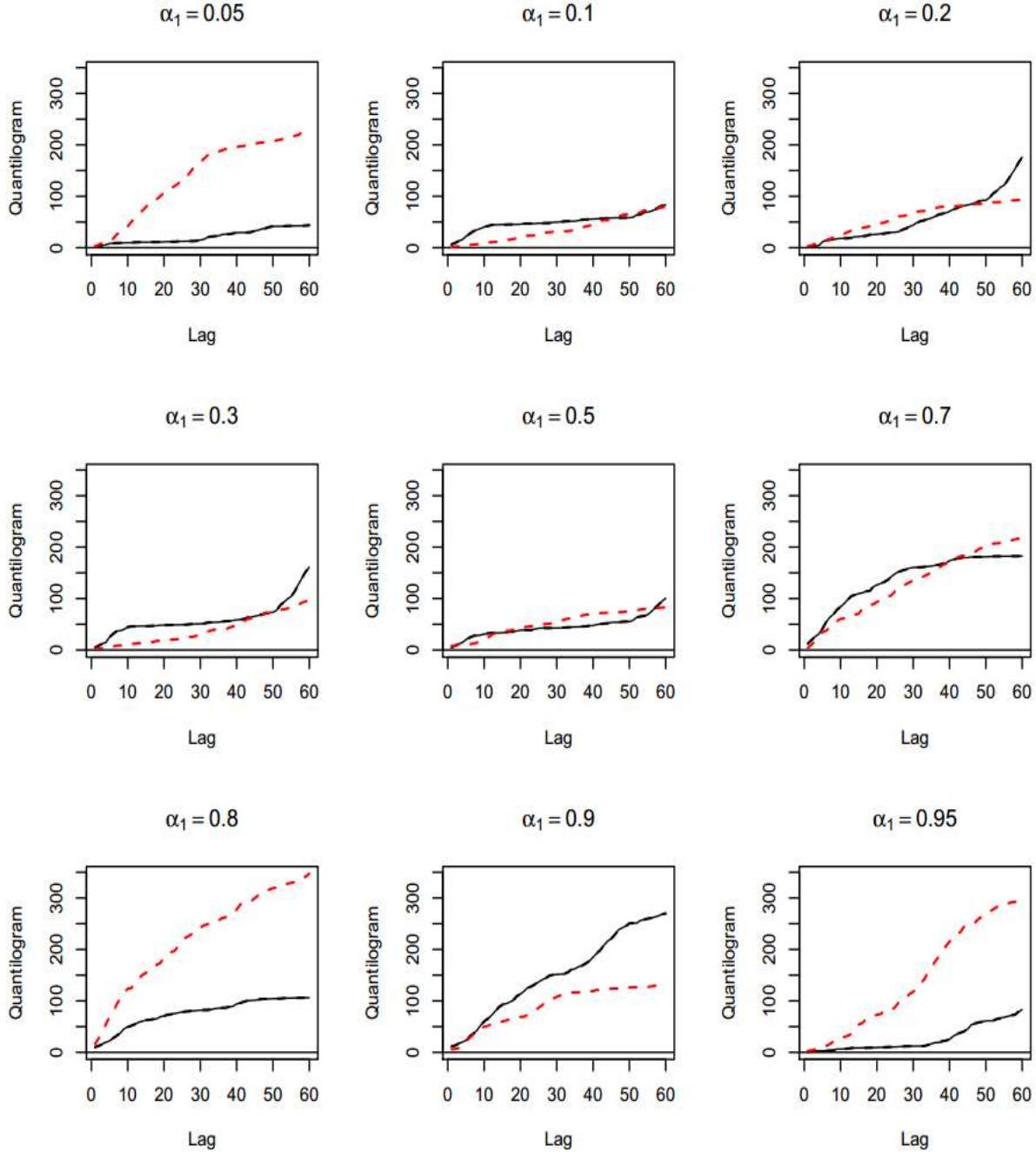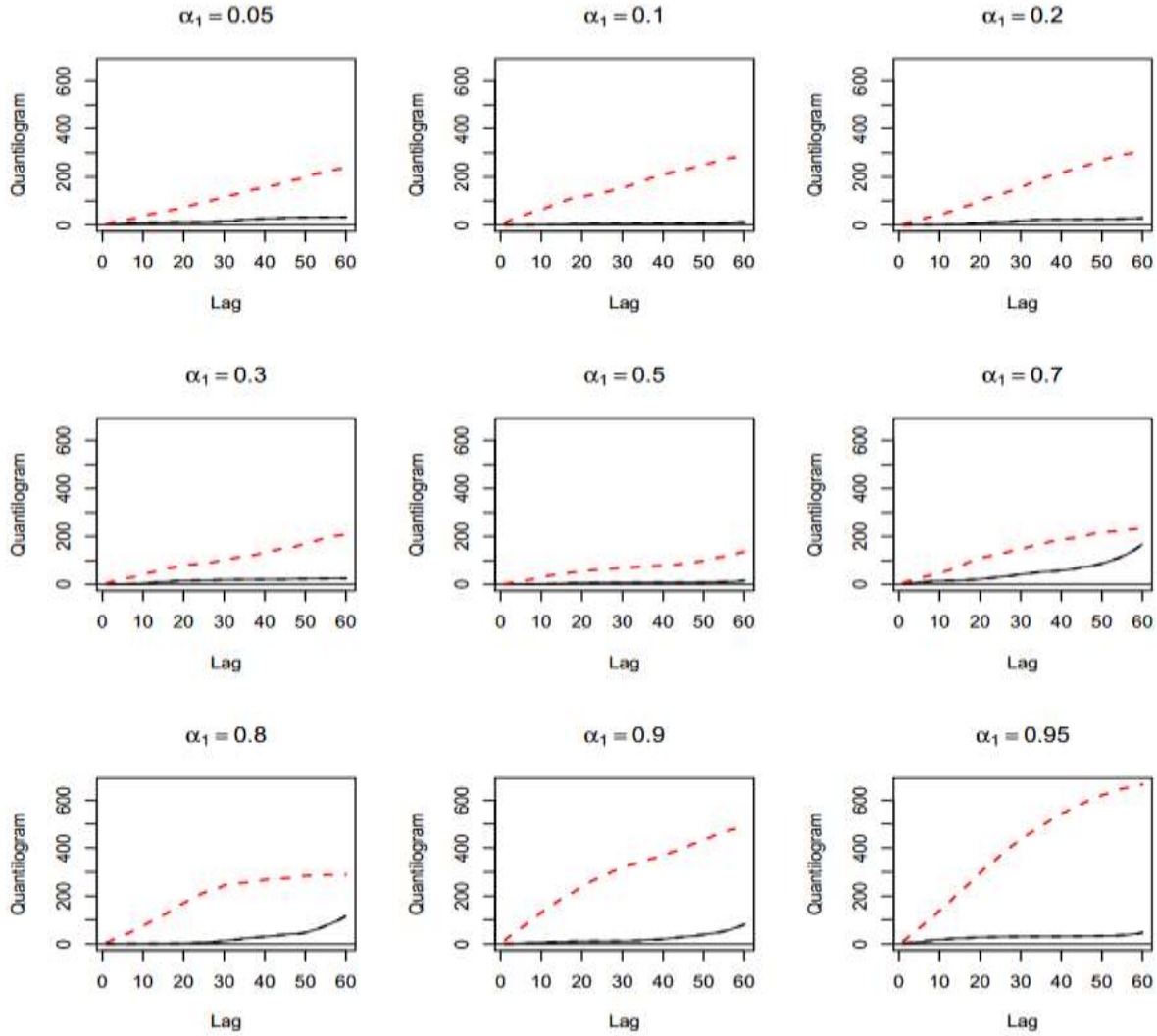
Fig. 1(b). Box-Ljung test statistic $\hat{Q}_\alpha^{(p)}$ for each lag p and quantile using $\hat{p}_\alpha(k)$, with α2 = 0.1. The dashed lines are the 95% bootstrap confidence intervals.

Figs. 2(a) and 2(b) are for the case in which the stock variance is in the median, i.e., q2 (α2) for α2=0.5. If the distributions of stock returns and the predictor are symmetric, the median return forecast will be equal to the mean return forecast. For α1 = 0.5 and α2 = 0.5, the cross quantilograms are insignificant for nearly all lags. The cross-quantilogram $\hat{p}_\alpha(k)$ for α1 = 0.2 and

21

0.3 is positive and significant for all lags. This finding means that when the GSFI is lower than the median, it is less likely to result in a very large negative loss for Bitcoin. The cross-quantilogram $\hat{p}_\alpha(k)$ for $\alpha_1 = 0.2$ and 0.3 is positive and significant for all lags. This finding means that when the GSFI is lower than the median, it is less likely to have a very large negative loss for Bitcoin. Fig. 2(b) shows the Box-Ljung test statistics for $\alpha_2 = 0.5$.

Fig. 2(a). The sample cross quantilogram $\hat{p}_\alpha(k)$ for α_2=0.5 to detect directional predictability from the GSFI to RBC. Bar graphs describe sample cross quantilograms, and lines are the 95% bootstrap confidence intervals.
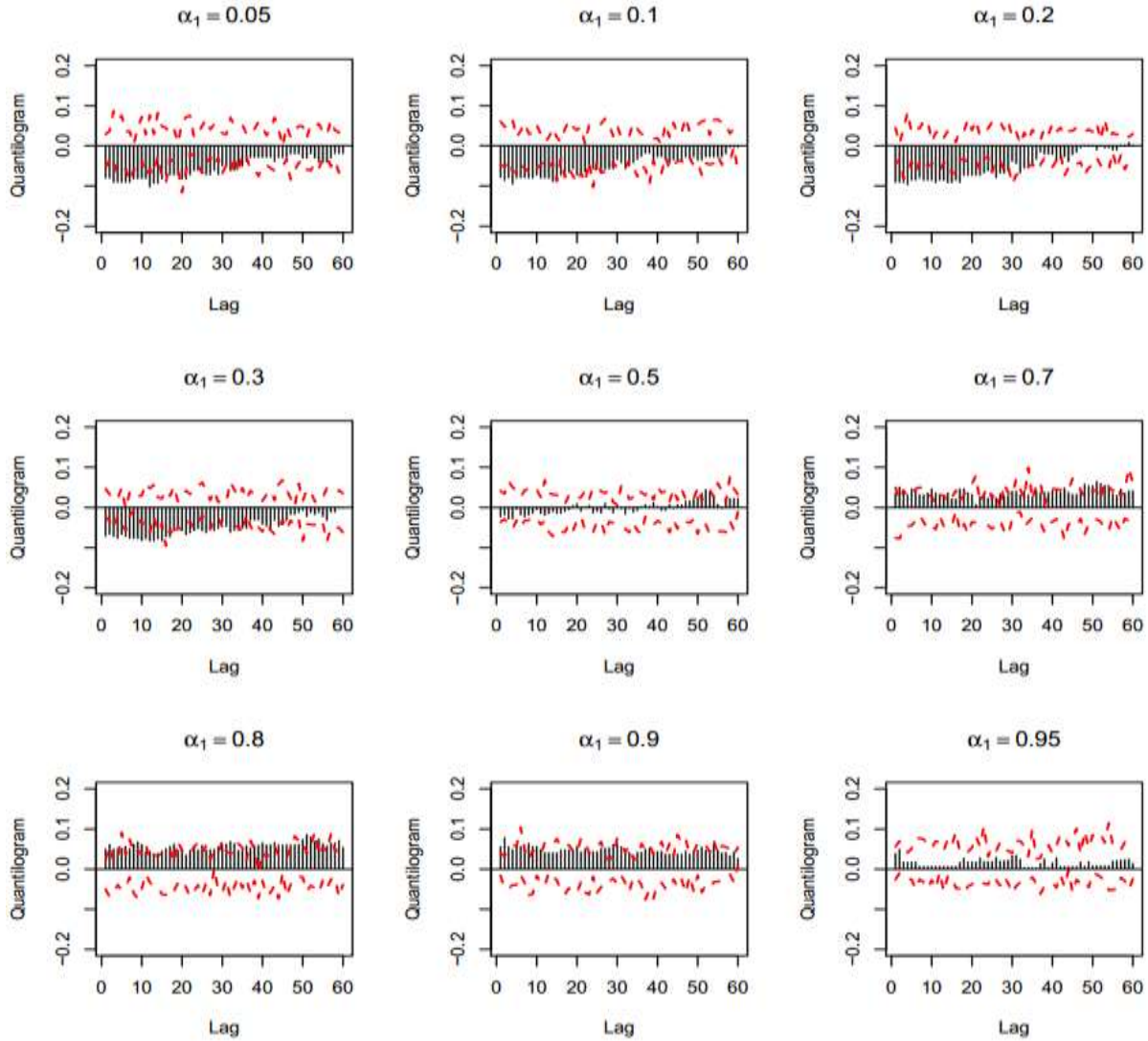
Fig. 2(b). Box-Ljung test statistic $\hat{Q}_{\alpha}^{(p)}$, for each lag p and quantile using $\hat{p}_{\alpha}(k)$ with α2=0.5. The dashed lines are the 95% bootstrap confidence intervals.

Figs. 3(a) and 3(b) are for the case in which stock variance is in the higher quantile, i.e., q2 (α2) for α2 = 0.9. Compared to the previous case of α2 = 0.5, the cross quantilograms have very different trends in addition to much larger absolute values. For α1 < 0.5, the cross quantilograms are negative and significant for approximately 40 days. This finding implies that when financial stress is higher than the 0.9 quantile, there is an increased likelihood of having very large negative losses to Bitcoin for a maximum of 40 days. For α1 = 0.9, the cross quantilograms are positive and significant for more than 60 days. This finding implies that when risk is very high (higher than the 0.9 quantile), there is an increased likelihood of having a very

large positive gain for the next 60 days. Fig. 3(b) shows that the Box-Ljung test statistics are significant for certain lags in most quantiles of Bitcoin returns, except for α1 = 0.5 and α1= 0.95.

Fig. 3(a). The sample cross quantilogram $\hat{p}_\alpha(k)$ for α2 = 0.9 to detect directional predictability from the GSFI to RBC. Bar graphs describe sample cross quantilograms, and lines are the 95% bootstrap confidence intervals.
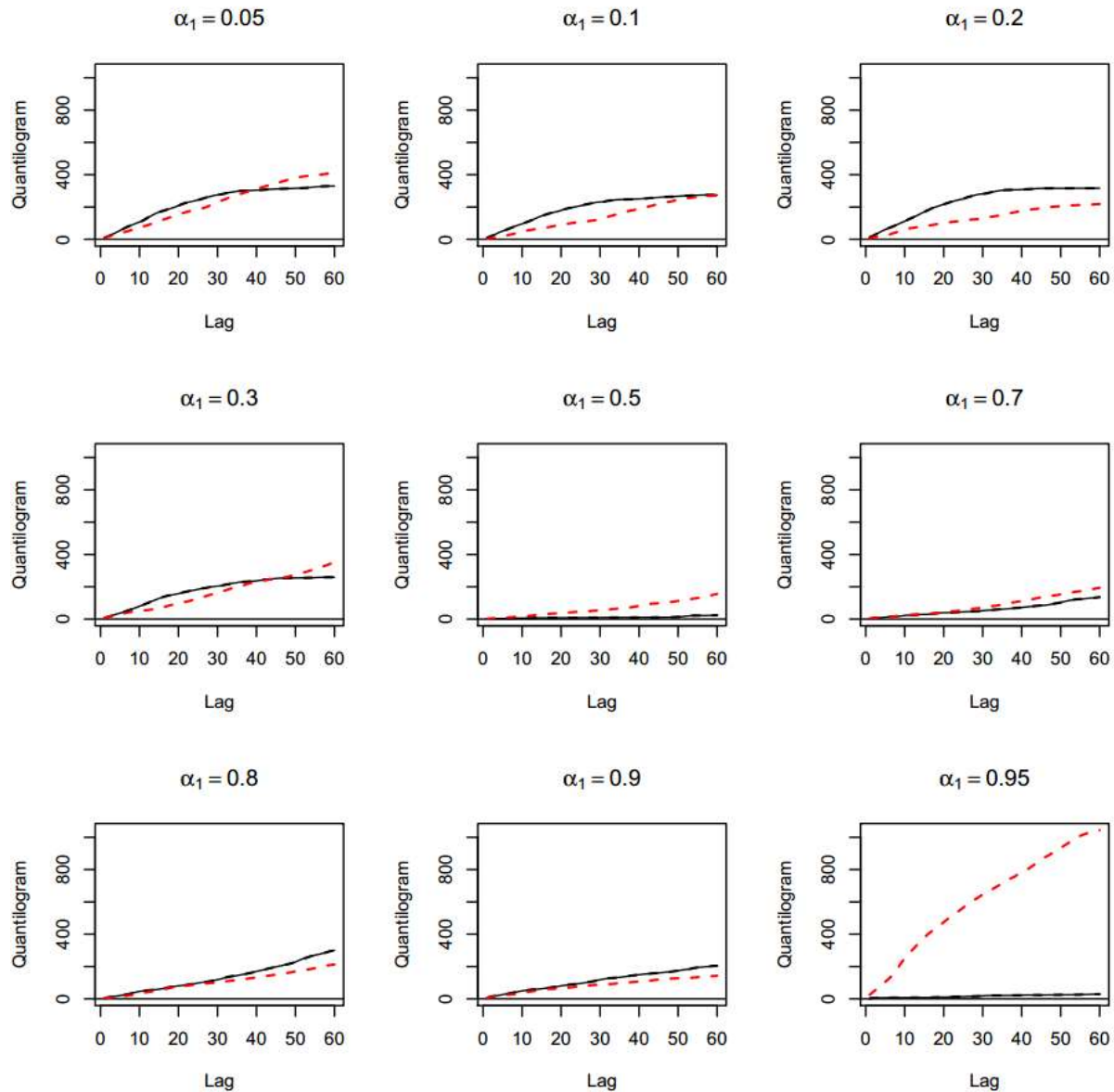
Fig. 3(b). Box-Ljung test statistic $\hat{Q}_\alpha^{(p)}$ for each lag p and quantile using $\hat{p}_\alpha(k)$, with α2 = 0.9. The dashed lines are the 95% bootstrap confidence intervals.

In summary, when global financial stress is in a higher quantile, in general, the absolute value of the cross-quantilogram is higher, and the cross-quantilogram is significantly different from zero for larger lags. Our results exhibit a more complete quantile-to-quantile relationship between financial stress and Bitcoin return and show how the relationship changes for different lags.

This evidence on Bitcoin's safe-haven property against global financial stress in certain quantiles from a predictive perspective adds to that reported by Bouri et al. (2017b) in general and Bouri et al. (2017a) in particular. The evidence can be explained by the well-documented view that Bitcoin is part of an alternative economy (Bouri et al., 2017), and its price formation depends on certain non-economic and non-financial factors and Bitcoin attractiveness indicators (Ciaian and Rajcaniova, 2016) such as the anonymity of payment transactions (EBA, 2014), use in illegal activities (Böhme et al., 2015), and computer-programming enthusiasts (Yelowitz and Wilson, 2015).

4 Conclusion

Initially introduced as an electronic payment system equivalent to cash that could be used nearly anonymously in e-commerce, Bitcoin has quickly gained ground as an investment asset. Although a great deal of attention has been devoted to the technological, cryptographic, and legal aspects of Bitcoin, empirical evidence of its economic and financial aspects, particularly its role as a safe haven against global financial stress, is relatively scarce. This paper addressed this void by examining the quantile dependence between Bitcoin and global financial stress, which is measured by the GFSI, from March 18, 2011, to October 7, 2016. Interestingly, the GFSI captures global stress better than the VIX because it aggregates 23 measures of stress covering factors that reflect deteriorating economic fundamentals and poorly functioning financial systems. Methodologically, we considered the quantile dependence using copula functions, given the inability of conventional methods to appropriately capture the dependence between Bitcoin returns and the GFSI, as the bivariate joint distribution is not normally distributed. This paper not only found evidence of right-tail dependence but also computed the inverse of the conditional copula distribution function as a necessary step to obtain the conditional quantile functions and examine the Granger causality in different quantiles; in addition, it showed that global financial stress strongly Granger-causes Bitcoin returns at the left tail (deficient performance) and the middle (average performance) but not at the right tail (superior performance) of the joint distribution. Furthermore, we focused on the quantile-to-quantile relation from a predictive perspective and revealed evidence of directional predictability from the GFSI to Bitcoin returns, suggesting Bitcoin's ability to act as a safe haven against global financial stress for approximately 60 days.

Overall, our findings support the literature on the valuable role of Bitcoin returns (Bouri et al., 2017a, 2017c; Brière et al., 2015; Dyhrberg, 2016a, 2016b; Ji et al., 2017) and extended it by showing the directional quantile dependence. This extension is important and useful to practitioners and policy-makers in an era of potentially high global financial stress. However, Bitcoin's possible benefits as a financial asset must be considered along with its associated volatility, which is documented in numerous studies (Pieters and Vivanco, 2017). It would also be premature to ensure that Bitcoin's role as a valuable investment will not be interrupted by a technological glitch. Future research can use the quantile dependence approach to more thoroughly examine Bitcoin's safe-haven property against conventional assets and commodities.

References

Balcilar, M., Bouri, E., Gupta, R., Roubaud, D., 2017. Can volume predict Bitcoin returns and volatility? A quantiles-based approach. Econ. Model. 64, 74–81.

Böhme, R., Christin, N., Edelman, B., Moore, T., 2015. Bitcoin: economics, technology, and governance. J. Econ. Perspect. 29, 213–238.

Bollerslev, T., Wooldridge, J.M., 1992. Quasi-maximum likelihood estimation and inference in dynamic models with time-varying covariances. Econometric reviews, 11(2), 143–172.

Bouri, E., Azzi, G., Dyhrberg, A.H., 2017c. On the return-volatility relationship in the Bitcoin market around the price crash of 2013. Economics 11, 1–16.

Bouri, E., Gupta, R., Tiwari, A.K., Roubaud, D., 2017a. Does Bitcoin hedge global uncertainty? Evidence from wavelet-based quantile-in-quantile regressions. Financ. Res. Lett. doi: 10.1016/j.frl.2017.02.009

Bouri, E., Molnár, P., Azzi, G., Roubaud, D., Hagfors, L.I., 2017b. On the hedge and safe haven properties of Bitcoin: is it really more than a diversifier? Financ. Res. Lett. 20, 192–198.

Brière, M., Oosterlinck, K., Szafarz, A., 2015. Virtual currency, tangible return: portfolio diversification with bitcoin. J. Asset Manag. 16, 365–373.

Ciaian, P., Rajcaniova, M., 2016. The digital agenda of virtual currencies: can Bitcoin become a global currency? Inf. Syst. e-Bus. Manag. 14, 883–919.

Dyhrberg, A.H., 2016a. Bitcoin, gold and the dollar – A GARCH volatility analysis. Finance Research Letters 16, 85–92.

Dyhrberg, A.H., 2016b. Hedging capabilities of bitcoin. Is it the virtual gold? Financ. Res. Lett. 16, 139–144.

Strunk Jr., W., White, E.B., 2000. The Elements of Style. Longman, New York.

Han, H., Linton, O., Oka, T., Whang, Y.-J., 2016. The cross-quantilogram: measuring quantile dependence and testing directional predictability between time series. J. Econom. 193, 251–270.

Hong, Y., Li, H., 2005. Nonparametric specification testing for continuous-time models with applications to term structure of interest rates. Rev. Financ. Stud. 18, 37–84.

Ji, Q., Bouri, E., Gupta, R., Roubaud, D., 2017. Network Causality Structures among Bitcoin and other Financial Assets: A Directed Acyclic Graph Approach, Report No 201729. University of Pretoria, Department of Economics, Pretoria.

Jiang, H., Su, J.-J., Todorova, N., Roca, E., 2016. Spillovers and directional predictability with a cross-quantilogram analysis: the case of U.S. and Chinese agricultural futures. J. Futur. Mark. 36, 1231–1255.

Koenker, R., Bassett Jr, G., 1978. Regression quantiles. Econometrica: journal of the Econometric Society, 33–50.

Lee, T.-H., Yang, W., 2014. Granger-causality in quantiles between financial markets: using copula approach. Int. Rev. Financ. Anal. 33, 70–78.

Lobato, I.N., 2001. Testing that a dependent process is uncorrelated. J. Am. Stat. Assoc. 96, 1066–1076.

Luther, W.J., Salter, A.W., 2017. Bitcoin and the bailout. Q. Rev. Econ. Financ. doi: 10.1016/j.qref.2017.01.009

Nelsen, R.B., 1999. An Introduction to Copulas. Springer, New York.

Ning, C., 2010. Dependence structure between the equity market and the foreign exchange market–a copula approach. J. Int. Money Finance 29, 743–759.

Patton, A.J., 2006. Estimation of multivariate models for time series of possibly different lengths. J. Appl. Econ. 21, 147–173.

Pieters, G., Vivanco, S., 2017. Financial regulations and price inconsistencies across Bitcoin markets. Inf. Econ. Policy 39, 1–14.

Politis, D.N., Romano, J.P., 1994. The stationary bootstrap. J. Am. Stat. Assoc. 89, 1303–1313.

Popper, N., 2015. Digital Gold: The Untold Story of Bitcoin. Penguin Books Limited, London.

Wang, Y.-C., Wu, J.-L., Lai, Y.-H., 2013. A revisit to the dependence structure between the stock and foreign exchange markets: a dependence-switching copula approach. J. Bank. Financ. 37, 1706–1719.

Weber, B., 2014. Bitcoin and the legitimacy crisis of money. Cambridge J. Econ. 40, 17–41.

Yelowitz, A., Wilson, M., 2015. Characteristics of Bitcoin users: an analysis of Google search data. Appl. Econ. Lett. 22, 1030–1036.

Appendix

Regime-dependent Copula

We further assume that the copula function is time-varying, depending on an unobservable state variable S_t.

$$C_{S_t} = \begin{cases} C_G(u,v) = \exp\left(-\left[(-\ln u)^{\theta_1} + (-\ln v)^{\theta_1}\right]^{1/\theta_1}\right) & \text{if } S_t = 1 \\ C_{RG}(u,v) = \exp\left(-\left[(-\ln(1-u))^{\theta_0} + (-\ln(1-v))^{\theta_0}\right]^{1/\theta_0}\right) & \text{if } S_t = 0 \end{cases} \tag{A1}$$

where u and v are the "probability integral transforms" of the GFSI and RBC. θ_1 is the parameter for the Gumbel copula, and θ_0 is the parameter for the rotated Gumbel copula.

The unobservable state variable S_t follows a two-state Markov chain. S_t transits between two states according to the transition probabilities.

$$P = \begin{bmatrix} P_{11} & P_{10} \\ P_{01} & P_{00} \end{bmatrix}$$

where $P_{ij} = \mathrm{P}(S_t = j \mid S_t = i)$ for $\{i,j\} \in \{1,0\}$. $\tag{A2}$

The bivariate density function of the above model is defined as

$$f_t^{TV}(x,y) = \sum_{i=0}^{1} \mathbf{P}(S_t = i) c_i(u,v) f_X(x) f_Y(y) \tag{A3}$$

where $c_i(u,v)$ is the copula under regime $i \in \{0,1\}$, i.e., $c_1(u,v) = \partial^2 C^C(u,v)/\partial u \partial v$ and $c_2(u,v) = \partial^2 C^{SC}(u,v)/\partial u \partial v$. Notice that we assume the copula functions are different under different regimes; however, the two marginal densities are the same across different regimes. The model with dependence switching enables us to discuss the asymmetric tail dependence and the transition between the left-tail dependence regime and the right-tail dependence regime. The log likelihood of the model of a parameter set $\Theta = \{\theta_c, \theta_X, \theta_Y\}$ with a given data $\mathbf{D}$ is

$$\mathbf{L}(\Theta) = \mathbf{L}_c(\theta_c) + \mathbf{L}_X(\theta_X) + \mathbf{L}_Y(\theta_Y)$$

where $\mathbf{L}_c(\theta_c)$ is the log likelihood of the copula density; $\mathbf{L}_X(\theta_X)$ and $\mathbf{L}_Y(\theta_Y)$ are the log likelihood of the two marginal densities.

$$\mathbf{L}_c(\theta_c) = \log\left[\sum_{i=0}^{1} \mathbf{P}(S_t = i) c_i(u,v)\right]$$
$$\mathbf{L}_X(\theta_X) = \log[f_X(x)]$$
$$\mathbf{L}_Y(\theta_Y) = \log[f_Y(x)] \tag{A4}$$

where $\theta_c = \{P_{00}, P_{11}, \theta_1, \theta_0\}$, θ_X and θ_Y are the parameter set for the two marginal models, respectively. Because of the structure of the log likelihood function, its three components can be optimized independently. Table A1 reports the results for the regime-dependent copula model; the result shows that the regime-switching effect is absent for our dataset (see Table A1), as P_{11} is exactly 1.000 with SD 0.000. Hence, the regime-switching is not suitable in our study. The Gumbel will always be chosen, and the rotated Gumbel will never be chosen. This finding can also be confirmed by smooth probability. This result is not surprising because Table 4 shows that there is no left-tail dependence for whatever copula is used, and there is very weak right-tail dependence only when the Gumbel copula is used.

Table A1. Estimation of the dependence-switching copula model.

		Value	SD
Gumbel	θ_1	1.014	0.013
Rotated Gumbel	θ_2	4.708	4.195
Regime Switching	P_{11}	1.000	0.000
	P_{22}	0.500	0.449
	Copula LV	-1.346	
	AIC	2.716	
	BIC	2.782	

Notes: θ_i is the shape parameter of the dependence-switching copula. "Copula LV" denotes the estimated log likelihood value for the copula function. P_{11} and P_{22} are two transition probabilities. SD denotes the standard deviation.